

Characteristics of Bubble Oscillations During Laser-Activated Irrigation of Root Canals and Method of Improvement

Matjaž Lukač,¹ Nejc Lukač,² and Matija Jezeršek ^{2*}

¹Jozef Stefan Institute, Ljubljana, Slovenia

²Faculty of Mechanical Engineering, University of Ljubljana, Aškerčeva 6, Ljubljana, 1000, Slovenia

Background and Objectives: Laser-activated irrigation of dental root canals is being increasingly used as its efficacy has been shown to be superior compared with conventional techniques. The method is based on laser-initiated localized fluid evaporation and subsequent rapid bubble expansions and collapses, inducing microfluid flow throughout the entire volume of the cavity. The irrigation efficacy can be further improved if optimally delayed “SWEEPS” double laser pulses are delivered into the canal. This study aims to show that the irrigation efficacy, as measured by the induced pressure within the canal, is related to the double pulse delay, with the maximal pressure generated at an optimal delay. The second aim is to find a method of determining the optimal delay for different cavity dimensions and/or laser parameters.

Study Design/Materials and Methods: Experiments were made in transparent models of root canals where Er:YAG laser ($\lambda = 2.94 \mu\text{m}$, pulse duration $t_p = 25$ or 50 microseconds, and pulse energies up to $E_L = 40 \text{ mJ}$) was used with a combination of cylindrical and conical fiber-tip geometries (diameters 400 and $600 \mu\text{m}$). High-speed photography ($60,000 \text{ fps}$) and average pressure measurements inside the canal were used for process characterization.

Results: The results show that a pressure amplification of more than 1.5 times occurs if the laser pulse delay approximately coincides with the bubble oscillation time. Correlations between normalized oscillation time and canal diameter for a wide range of laser pulse energies ($R^2 = 0.96$) and between the average pressure within the canal and the bubble oscillation periods ($R^2 = 0.90$) were found. A relationship between the bubble oscillation time and the diameter of the treated cavity was found depending on the bubble oscillation time in an infinite fluid reservoir.

Conclusions: The bubble oscillation time within a constrained volume can be determined based on the known oscillation time in infinite space, which offers a fast and simple solution for optimization of the laser parameters. These findings enable determination of optimal conditions for shock wave generation, and improvement of root canal irrigation at the same dose of laser energy input, leading

to improved treatment efficacy and safety. Lasers Surg. Med. © 2020 The Authors. *Lasers in Surgery and Medicine* published by Wiley Periodicals, Inc.

Key words: laser-induced cavitation; laser-activated irrigation; Er:YAG laser; cavitation bubble; constrained environments; root canals

INTRODUCTION

Laser-activated irrigation (LAI) of root canals is a procedure, where elimination of pathogenic substances from the root canal system is driven by laser-induced cavitation [1]. Due to the complex, three-dimensional anatomy of root canals, a significant portion of canal wall surfaces (20–60%) remain un-instrumented with standard mechanical techniques [2]. Furthermore, mechanical instrumentation creates a smear layer along with an accumulation of surface debris [3]. To remove the smear layer and debris produced during instrumentation, as well as eradicate potential pathogens, irrigation is required [4].

Numerous techniques have been introduced to improve the efficacy of standard syringe root canal irrigation [5–9]. One such technique is a LAI, which generates a micro-cavitation within the irrigant inside the root canal system [10–13].

This is an open access article under the terms of the Creative Commons Attribution-NonCommercial-NoDerivatives License, which permits use and distribution in any medium, provided the original work is properly cited, the use is non-commercial and no modifications or adaptations are made.

Conflict of Interest Disclosures: All authors have completed and submitted the ICMJE Form for Disclosure of Potential Conflicts of Interest and have disclosed the following: Two of the authors (Matjaž Lukač and Nejc Lukač) are affiliated also with Fotona, d.o.o.

Contract grant sponsor: Ministry of Education, Science and Sport, Slovenia; Contract grant numbers: L3-7658, P2-0392; Contract grant sponsor: Fotona d.o.o.

*Correspondence to: Dr. Matija Jezeršek, Faculty of Mechanical Engineering, University of Ljubljana, Aškerčeva 6, Ljubljana 1000, Slovenia. E-mail: matija.jezersek@fs.uni-lj.si

Accepted 10 February 2020

Published online 17 February 2020 in Wiley Online Library

(wileyonlinelibrary.com).

DOI 10.1002/lsm.23226

Due to the high absorption of Erbium lasers with a wavelength around $3\ \mu\text{m}$ in the irrigant, the LAI concept initiates the rapid formation of a vapor bubble at the fiber tip (FT) while it is immersed in the irrigant [14–16]. This triggers a turbulent fluid movement within the entire canal, leading to improved chemomechanical debridement [13,17–20]. An example of LAI is the photon-induced photoacoustic streaming method, performed with a single Er:YAG laser super short pulse with a duration of 50 microseconds [16,18,19].

The principle behind the cavitation phenomena is the difference in compressibility between a gas and a liquid. The volume of liquid hardly changes in response to a variation in pressure, whereas the volume of the gaseous interior of a bubble can change dramatically. Any contraction or expansion of the bubble is inevitably accompanied by a displacement of an equal volume of the much denser surrounding liquid. As a result, a strong bubble response in combination with the compressible interior can provide not only localized fluid motion, but also a tremendous focusing of liquid kinetic energy. Of particular interest for cleaning are the shock waves that may form during the bubble's collapse. These shock waves spread through the volume at supersonic speeds and interact disruptively with the surrounding environment (e.g., cavity walls). These waves are not only very effective in removing any contamination from the cavity surfaces, but can also kill bacteria, leading to a partial or complete disinfection of the treated cavity. Significant inactivation of the *Escherichia coli* bacteria has been reported in Šarc et al. [21] where cavitation has been induced hydrodynamically.

In an infinite liquid, a shock wave is emitted during the accelerated contraction of the bubble cavity. However, in a confined environment such as an endodontic access opening, a free expansion of the bubble is not possible, and the expansion and contraction of the bubble is slowed down by the added resistance to flow due to the impermeability and the no-slip condition on the cavity's surface. This process slows down the dynamics of the bubble's expansion and implosion compared with a free liquid situation, and the period of the bubble's oscillations can be significantly extended up to ten times [22].

For this reason, a SWEEPS (Shock Wave Enhanced Emission Photoacoustic Streaming) technique has been developed, as a solution for improving the efficacy of LAI in narrow endodontic cavities [13,20,22–24]. The SWEEPS shock wave enhancing technique consists of delivering a properly timed second laser pulse during the collapse phase of the primary bubble generated by a first laser pulse. The growth of the second cavitation bubble accelerates the collapse of the first cavitation bubble, leading to a violent collapse, during which shock waves are emitted. The shock waves are generated not only by the accelerated collapse of the primary cavitation bubble but also by the simultaneous collapse of the accompanying smaller secondary bubbles deeper within the endodontic space, potentially increasing the cleaning and disinfecting efficacy of laser-induced irrigation to a significant degree.

As the optimal delay between the two SWEEPS laser pulses depends on the cavitation bubble's oscillation period, this presents a challenge. Namely, for the same laser parameters the bubble oscillation period and consequently the optimal SWEEPS delay varies with the size and shape of each individual endodontic access opening. For this reason, it is important to understand how bubble dynamics changes in constrained endodontic spaces.

In this research, we first studied how the cavitation bubble size and oscillation period depend on the diameter of a cylindrical model of the endodontic cavity. We then measured the dependence of the internal pressures generated in a root canal model on the bubble oscillation period. Finally, we studied the dependence of the generated pressures on the SWEEPS pulse pair temporal separation.

MATERIALS AND METHODS

Experimental System

The experimental system for studying characteristics of cavitation bubbles as generated by single or dual laser pulses in constrained cavity is shown in Figure 1. The simulated transparent root canal models of different shapes and sizes were submerged 4 mm deep under the water level of a large reservoir ($150 \times 100 \times 100\ \text{mm}$). The cavitation inside the canal was induced using an Er:YAG laser (LightWalker; Fotona d.o.o., Slovenia, $\lambda = 2.94\ \mu\text{m}$) equipped with a dental handpiece (H14, Fotona d.o.o.) optically coupled with an interchangeable FT.

A high-speed camera (Fastcam SA-Z; Photron, Japan) with 1:1 magnification lens (Sigma APO Macro, Sigma corporation, Japan, $f = 180\ \text{mm}$, F2.8) was used to observe cavitation dynamics within a simulated root canal. Its frame rate at full resolution ($1,024 \times 1,024$ pixels) is 20,000 fps. We typically used a frame rate 60,000 fps at reduced resolution of $300 \times 1,024$ pixels, and shutter time 200 nanoseconds. In order to see a sharp boundary between the bubble and surrounding liquid, we used back illumination with one 50,000 lumen LED reflector (XHP 50000; X-LED technology,

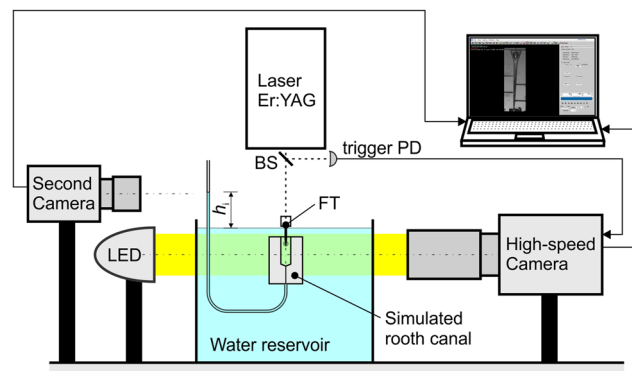


Fig. 1. Experimental system. A high-speed camera captures laser-induced bubble dynamics inside of simulated root canal. A second camera measures pressure within the root canal based on water column height (h_1) inside the tube connected to the opening of a simulated root canal. BS, beam splitter; FT, fiber tip; LED, light-emitting diode; PD, photodiode.

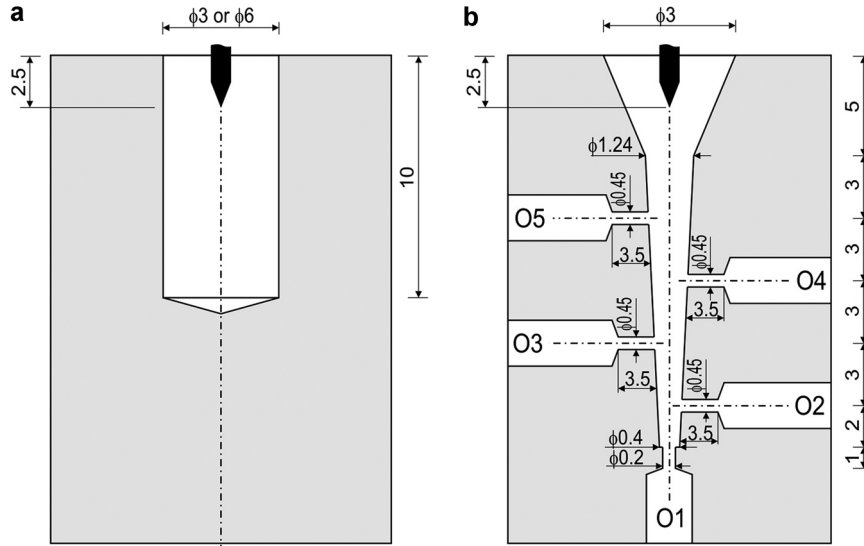


Fig. 2. Geometry of simulated root canals. (a) cylindrical shape, where two different diameters were used (3 or 6 mm). (b) Conical shape for measuring pressures at different locations within the canal. The lateral constrictions ($i=2-5$) had approximate diameter $r_i=0.225$ mm and lengths $l_i=3.5$ mm, while the vertical (apical) constriction's approximate dimensions were $r_1=0.1$ mm and $l_1=1$ mm. The location of the laser fiber tip in the access cavity is represented by the tapered black tip.

Netherlands). The camera was triggered by laser pulses using a trigger photodiode, which detects laser light partially reflected by a beam splitter.

The simulated root canals were made from transparent polymethyl methacrylate blocks ($15 \times 15 \times 30$ mm) in three shapes (see Fig. 2): cylindrical with diameter 3 and 6 mm and conical with side openings. The cylindrical canals were used for measuring the bubble's maximal radius (R_B) characterizing the bubble's maximal volume (V_{max}), and its oscillation period (T_B), while the conical canal was used for measuring laser-induced pressures at different regions inside the canal.

Measurement of the bubble size and oscillation period was based on analyzing the image sequences acquired by the high-speed camera. A typical example is shown in Figure 3, where the yellow ellipse (at 170 microseconds) marks the image with the maximal bubble size and the yellow rectangle (at 380 microseconds) marks the moment of the first collapse.

As the bubble shape is not spherical due to confined boundary effects, an approximation of an ellipse on the bubble boundary is first made. Then, under the assumption that the bubble is axisymmetric, the mean bubble radius is calculated as:

$$R_B = \sqrt[3]{a^2c} \quad (1)$$

where a and c are the radii and height of a spheroid defined by an approximated ellipse.

The oscillation period T_B is determined simply by finding the image and the corresponding time where the first collapse occurs.

The pressure measurement was based on observation of water column heights inside of each tube connected to the five openings (O1...O5) located at different depths of the conically shaped root canal (see Fig. 2b). The tubes with an internal diameter of 1.6 mm were ended with a vertical section extending 10 cm above the water level. A second camera (Chameleon3, 1.3 MP; PointGrey, Richmond, Canada) was used for measuring the water level heights simultaneously for all five water columns, with a resolution of 0.25 mm and frequency of 10 measurements per second. A custom computer program was developed for video data processing in order to detect the water level in each tube and store the measured values, h_i , into a data file.

During simulated irrigation conditions, laser pulses were delivered through the FT into the access cavity at a constant repetition rate of $f=20$ Hz. When laser radiation was turned on, the fluid columns h_i started to rise as a result of the increased pressure within the root canal, until they reached their individual equilibrium heights, h_{oi} (see Fig. 3), which was reached when both flows became equal and consequently the height stopped changing. Because of this pressure difference, the height of the water columns started to decrease immediately after laser radiation was turned off. For column heights below 20 mm, as was the case during our measurements, the height decrease rates (v_i) in the absence of laser radiation were found to be approximately linearly dependent on the column height for all columns, $v_i(h_i) = -k_i \times h_i$. This allowed the downward (Q_{di}) and upward (Q_{ui}) average fluid flows at the equilibrium to be calculated from:

$$Q_{ui} = Q_{di} = k_i \times h_{oi} \quad (2)$$

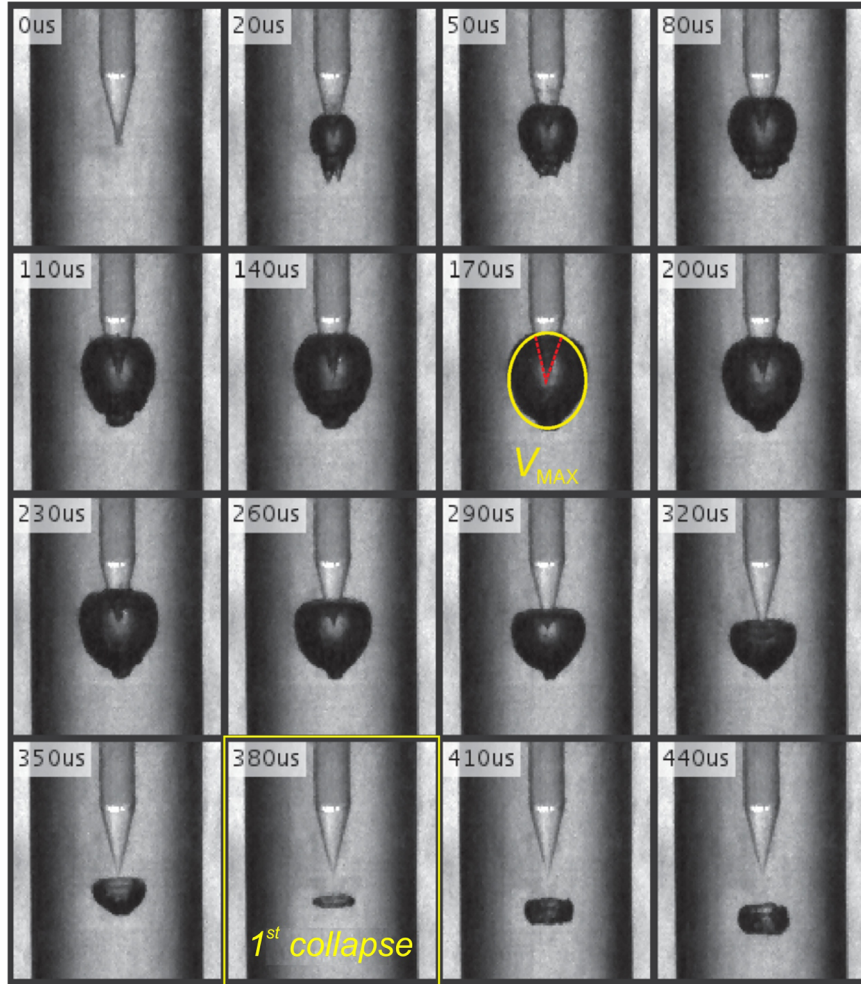


Fig. 3. Typical sequence of acquired images during laser bubble generation inside the cylindrical canal.

The pressure differences (P_i) between the two ends of the narrow constrictions were then calculated using the Hagen–Poiseuille equation defining the pressure difference in an incompressible and Newtonian fluid that is required to result in a laminar flow rate Q through a cylindrical pipe [25,26]:

$$P_i = \mu Z_i Q_{ui} \tag{3}$$

Here, μ is the fluid's viscosity ($\mu_{\text{water}} = 8.90 \times 10^{-4}$ Pa·s at 25°C), Q_{ui} is the measured downward average fluid flow at the equilibrium stage, and $Z_i = 8l_i/(\pi r_i^4)$ is the constriction's flow resistance where r_i is the radius and l_i is the length of the constriction. It is to be noted that at the equilibrium, that is, when during laser irradiation the height of the columns stops rising (see Fig. 4), the pressure difference (P_i) resulting from the water column's weight, that is, pushing the liquid back into the root canal, and the root canal's internal pressure ($P_{\text{int-}i}$) resulting from the laser-generated bubble dynamics, that

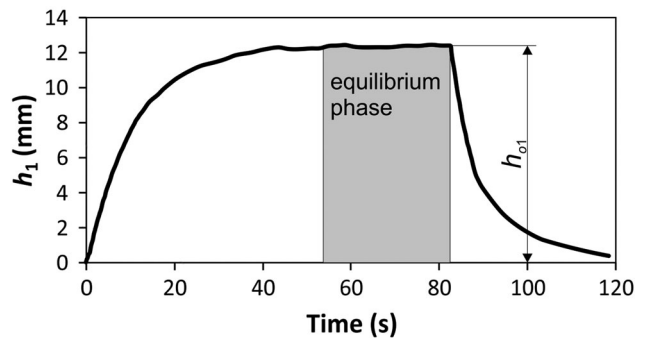


Fig. 4. Typical temporal evolution of the water column's height during and after laser radiation. The shown example is for the opening O1. The equilibrium phase, where downward and upward flows are equal, is marked as gray and h_{oi} is measured as an average of this interval.

is, pushing the liquid out of the root canal, become equal and therefore $P_{\text{int}-i} = P_i$.

This technique is advantageous in comparison with other pressure measurement techniques such as with piezo transducers or fiber-optic pressure sensors, as it allows simultaneous pressure measurements at different closely spaced locations (see Fig. 2b). With our technique, the number of simultaneous measurement locations is limited only by the camera's measuring range.

The average pressure within the entire canal (P_{avg}) was calculated as $P_{\text{ave}} = (P_1 + P_2 + P_3 + P_4 + P_5)/5$.

Experiments

Analysis of the bubble size and oscillation period in relation to the diameter of the simulated canal cavity was done in cylindrical models with diameters of 3 and 6 mm. In addition, we also measured bubble dynamics in a water reservoir without a canal to simulate infinite space. Single Er:YAG laser pulses of duration $t_p = 50$ microsecond and pulse energies $E_L = 5, 7.5, 19, 26,$ and 34 mJ were used. A flat-ended 14 mm long cylindrical FT of $400 \mu\text{m}$ diameter (Fotona Flat Sweeps400, Sigma corporation) was used.

Pressure measurements were made in a conical root canal using single laser pulses of durations $t_p = 25$ and 50 microseconds, and pulse energies $E_L = 10, 20, 30,$ and 40 mJ. Each combination of pulse duration and energy was used on four FT (all were 14 mm long): a flat-ended cylindrical FT of $400 \mu\text{m}$ diameter (Fotona Flat Sweeps400), a flat-ended cylindrical FT of $600 \mu\text{m}$ diameter (Fotona Flat Sweeps600), a conically-ended (with subtended angle of 34°) cylindrical FT of $400 \mu\text{m}$ diameter (Fotona Radial Sweeps400) and a conically-ended (with subtended angle of 34°) cylindrical FT of $600 \mu\text{m}$ diameter (Fotona Radial Sweeps600). Bubble oscillation times T_B were measured with a high-speed camera during the pressure measurements.

Finally, the dependence of the temporal separation of the SWEEPS dual pulses (T_p) on the generated pressures was measured using two FT geometries (Radial Sweeps400 and Radial Sweeps600). The sum of the energies of the first and second laser pulse in the SWEEPS pulse pair was 20 ± 4 mJ and the energy of the first pulse was $E_L = 12 \pm 2$ mJ. The duration of each laser pulse was $t_p = 25$ microseconds. The temporal separation time T_p was varied in intervals from 220 to 570 microseconds with increments of 20 or 40 microseconds. Coarser increments were used at the beginning and at the end of the interval, where we didn't expect significant pressure amplification.

In all cases, the laser FT endings were positioned 2.5 mm deep into the access cavity, according to the photon-induced photoacoustic streaming protocol [18]. An XYZ micrometer positioning stage and a camera with the optical resolution of 0.1 mm were used in order to assure repeatable FT positioning. In all experiments, at least seven measurements were repeated for each combination of parameters. Average values and standard deviations were then calculated and presented in the results.

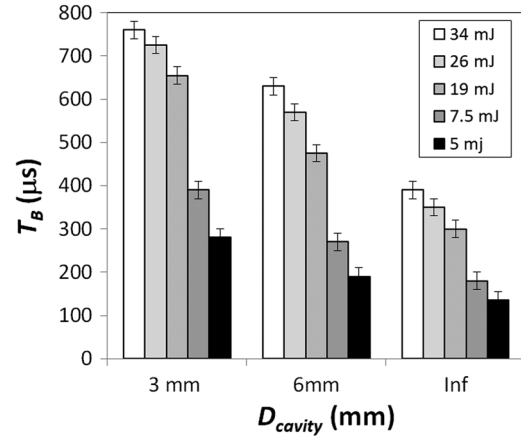


Fig. 5. Dependence of the cavitation bubble oscillation period (T_B) on the diameter D_{cavity} (3 and 6 mm and “Infinite”) of the cylindrical cavity for single Er:YAG laser pulses of duration $t_p = 50$ microseconds, and pulse energies $E_L = 5, 7.5, 19, 26,$ and 34 mJ. A flat-ended fiber tip with $400 \mu\text{m}$ diameter (Flat Sweeps400) was used.

RESULTS

Figure 5 shows the measured dependence of the bubble oscillation period T_B on the diameter D_{cavity} of the cylindrical cavity model for Er:YAG laser pulse energies E_L in the range from 5 to 34 mJ.

The maximal bubble radiuses R_B , corresponding to the bubble oscillation periods shown in Figure 5 above are depicted in Figure 6.

The temporal rate of the bubble's growth and collapse as represented by R_B/T_B is shown in Figure 7. As can be seen, the rate of the bubble's collapse is by a factor of about three or two times slower in cylindrical cavities of diameter 3 and 6 mm, correspondingly, in comparison with the rate of the bubble's

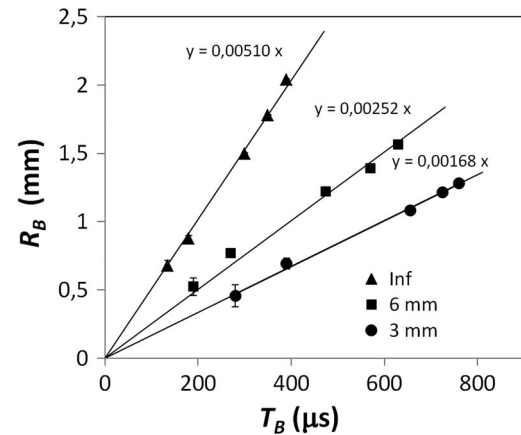


Fig. 6. Maximal bubble radiuses R_B corresponding to the bubble oscillation periods depicted in Figure 5, for different diameters of the cylindrical cavity (3 and 6 mm, and “infinite”). The full lines represent linear fits to the data.

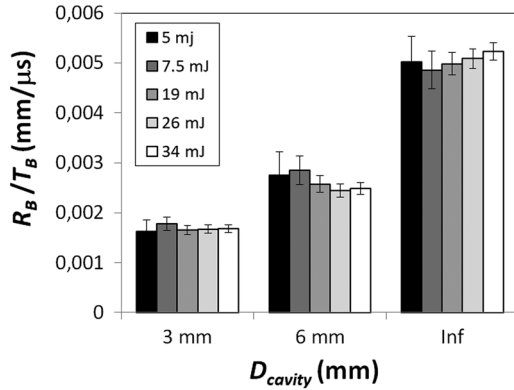


Fig. 7. Bubble growth and collapse rates, represented by the ratio of the bubble's maximal radius and oscillation period, R_B/T_B , for the data depicted in Figure 5. The rate of collapse in $D_{cavity} = 6$ mm and $D_{cavity} = 3$ mm is slower by approx. a factor of two or three, correspondingly, compared with an infinite reservoir.

collapse in an unconstrained infinitely large fluid reservoir.

Figure 8 shows the relationship between the measured average pressures in the root canal model and the corresponding cavitation bubble oscillation periods, T_B , as generated by single Er:YAG laser pulses. The eight data points for each of the FT geometries used represent the results as obtained for pulse durations $t_p = 25$ and 50 microseconds and laser pulse energies $E_L = 10, 20, 30$, and 40 mJ.

Finally, Figure 9 shows the dependence of the pressures along the depth of the root canal, as a function of the temporal separation (T_p) of the SWEEPS dual pulses for two FT geometries, Radial Sweeps400 (Fig. 9a) and Radial Sweeps600 (Fig. 9b). For each FT

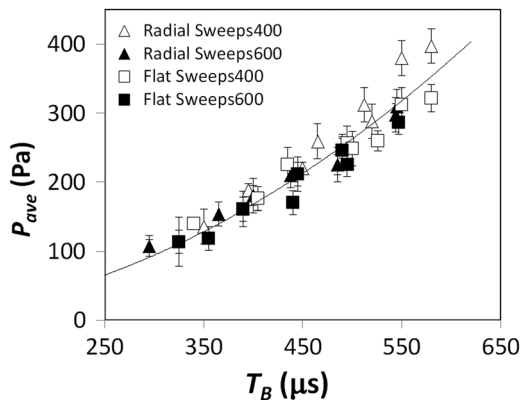


Fig. 8. Measured relationship between average fluid pressures, P_{ave} within a model root canal and the bubble oscillation periods T_B , as generated by single Er:YAG laser pulses. The eight data points for each of the fiber tip geometries used represent the results as obtained for pulse durations $t_p = 25$ and 50 microseconds and laser pulse energies $E_L = 10, 20, 30$, and 40 mJ. The full line represents a square ($\propto T_B^2$) fit to the data with $R^2 = 0.90$.

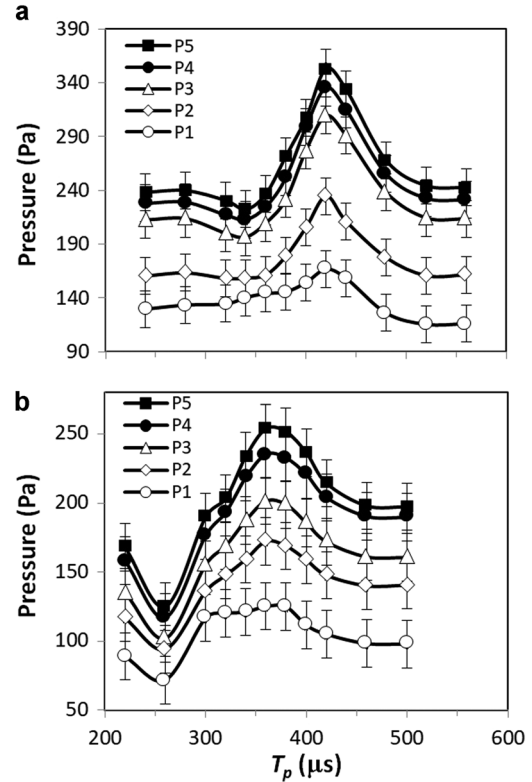


Fig. 9. Dependence of the internal pressures along the length of the root canal, as a function of the temporal separation (T_p) of the X-SWEEPS dual pulses for two fiber tip geometries: (a) Radial 400 μm and (b) radial 600 μm . The pressure maximums correspond approximately to the oscillation periods of $T_B = 405 \pm 15$ microseconds for the 400 μm fiber tip and $T_B = 365 \pm 15$ microseconds for the 600 μm fiber tip.

geometry, the maximum pressure is located approximately at the pulse separation being equal to the oscillation period of the primary bubble as generated by the first pulse of the SWEEPS pulse pair. The oscillation periods were $T_B = 405 \pm 15$ microseconds for the 400 μm FT and $T_B = 365 \pm 15$ microseconds for the 600 μm FT.

DISCUSSION

A challenge involved in using the innovative SWEEPS technique is that the separation between the two laser pulses (T_p) should not deviate substantially from the optimal separation ($T_{p,opt}$). This was shown in Lukač and Jezeršek [22], where the optimal separation time ($T_{p,opt}$) for the enhanced shock wave generation was found to be the pulse repetition time where the subsequent bubble starts to develop near the end of the first bubble's period (T_B). Our pressure measurements are in agreement with these findings since the pulse separation time where the largest pressure increase was observed to approximately coincide with T_B (Fig. 8), that is, when the start of the rapid growth of the second bubble at $t \approx T_B$ coincides with the collapse of the first bubble toward the end of its oscillation period T_B . It is to be noted that during its

development, the first bubble moves downwards and collapses at about half of its maximal diameter away from the FT (see Fig. 3), thus providing sufficient space for the growth of the second bubble.

When the same device is intended to be used for cleaning differently sized cavities, and/or with different device parameters (laser pulse energy or FT geometry, for example), obtaining a “SWEEPS” type enhancement poses a challenge, since as shown in Figure 5 the bubble oscillation time (T_B) and consequently the optimal pulse repetition time ($T_{p,opt}$) depend critically on these conditions, being longer for smaller cavities and/or for higher laser pulse energies.

The main reason for this dependence is related to the confined cylindrical cavity where free expansion of the bubble in a lateral direction is not possible, and hence the fluid is pushed forward and backward in the canal. The pressure inside the bubble remains high for a longer time, as it has to fight against the resistance of the water, which has to be displaced in the small canal. This process slows down the dynamics of expansion and implosion, and introduces additional losses compared with a free space situation. In the cavity, the lateral and forward bubble expansion is limited by the cavity wall, while the backward expansion is blocked by the fiber, making the lumen of the cavity even smaller. This results in a two- or three-times slower bubble growth and collapse rate (R_B/T_B) compared with an infinite reservoir (see Fig. 7). Consequently, no shock waves were observed in our experiments for $D_{cavity} = 3$ and 6 mm, which is in agreement with [22]. More important, in the free reservoir, shock wave emission was present during the bubble's collapse [27].

Figure 6 also shows a linear relationship between T_B and R_B , which indicates that a Rayleigh model for bubble oscillation time [28] can also be used for confined cavities if dependence on the cavity diameter (D_{cavity}) is introduced:

$$T_B = \beta(D_{cavity}) 1.83R_B \sqrt{\frac{\rho_\infty}{p_\infty - p_v}} \quad (4)$$

where coefficient β , which is only a function of the cavity diameter D_{cavity} , is added to the Rayleigh equation. In addition, ρ_∞ is the liquid density, p_∞ is the liquid pressure, and p_v is the vapor pressure inside the bubble at its maximal radius R_B . Since the bubble oscillation time T_B gets shorter with decreasing cavity diameter, comparing with the case of infinite space ($T_{B,inf}$), it can be shown that the measured data for different laser pulse energies can be well-described by a function:

$$\beta(D_{cavity}) = \frac{T_B}{T_{B,inf}} = 1 + \frac{K}{D_{cavity}} \quad (5)$$

where K is a fitting parameter. Good correlation between the measurements and model is demonstrated in Figure 10, where the obtained ratio $T_B/T_{B,inf}$ is found to be

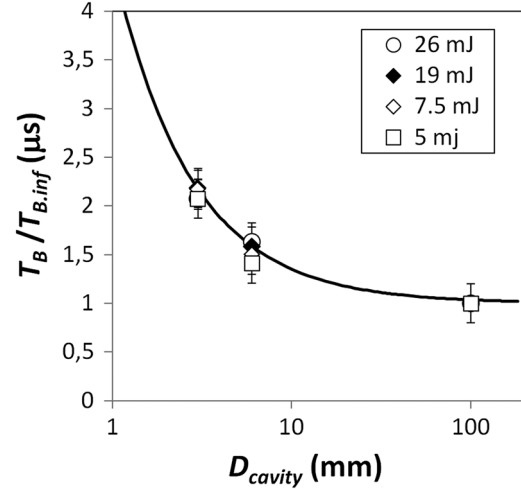


Fig. 10. Bubble oscillation times, T_B , normalized to the free oscillation times $T_{B,inf}$ in an infinite reservoir, as a function of the cavity diameter D_{cavity} . The fit to the data points represents a function, $T_B/T_{B,inf} = 1 + K/D$, where $K = 3.52$ mm, with the statistical coefficient of determination $R^2 = 0.96$.

approximately independent of the laser pulse energy E_L , with the best-fit obtained for the parameter $K = 3.52$ mm and the statistical coefficient of determination $R^2 = 0.96$.

It is to be noted that the above relationship appears to be applicable not only to bubbles generated by Er:YAG laser pulses, but to bubble generation by any energy device means.

In endodontic root canal treatments, the endodontist makes an access cavity in the crown of the tooth in order to enable cleaning and shaping of the interior of each of its root canals. It is to be noted that in endodontics the cavitation bubble dynamics is determined mainly by the dimensions of the access cavity in the vicinity of the FT, and not by the size, curvature, and complexity of the root canal beneath the cavity. Clinically, the size and shape of the lateral surface of the access cavity depends on the tooth type, the patient, and also on the endodontist's skill and preference. For upper central and lateral incisors, the shape of the lateral surface is typically circular. For the first, second, and third molars the shape of the lateral surface is approximately quadrangular with rounded corners. And for other teeth, the shape of the lateral surface is approximately elliptical. The size and shape of the lateral surface is typically described by the mesio-distal (minor) D_{min} , and buccolingual (major) D_{max} cavity diameter, the diameters being in the range of about 0.5–7 mm. Our preliminary measurements on extracted teeth indicate that Equation (4) can be used also in clinical endodontics, provided that the diameter D_{cavity} in Equation (5) is taken as the average diameter of the access cavity ($D_{ave} = (D_{min} + D_{max})/2$), but further research needs to be carried out to confirm this conclusion.

Our results also show that there is an approximately square relationship between the bubble oscillation period and the generated average pressure within a cavity

(Fig. 8), where $P_{ave} = 0.001 T_B^2$ with $R^2 = 0.90$. This offers the possibility of optimizing device parameters, such as laser wavelength, laser pulse energy, pulse duration, or FT geometry, by simply comparing measured bubble oscillation periods within the same cavity for all considered device parameters. The parameter combination, which results in the longest bubble oscillation period will be most effective also for pressure generation.

In a clinical setting, the access chamber is during the treatment kept filled-up using a syringe. In our experiment, the model root canal was for simplicity and constancy of experimental conditions, immersed in a water bath in order to avoid the need for replenishment of the irrigant due to the irrigant being pushed out of the model by the generated bubbles. This does not affect the conclusions of our experiment since in a separate research [22] it was shown that the bubble oscillation time is almost invariant to the FT depth within the irrigant reservoir.

In addition to irrigation efficacy, the patient's safety and the reduction of post-operative pain must also be considered. One of the questions involving SWEEPS is whether cavitation effects can extend also to the area outside of the apical constriction or outside of a perforated tooth. In our study, cavitation was observed only inside of the root canal, with no cavitation detected in the transparent tubes outside of any of the root canal model openings. We attribute this observation to the fact that cavitation occurs only if the liquid volume is subjected to sufficiently low pressure, and that due to the high flow resistance of the root canal narrow openings the pressure difference between the root canal and the surrounding falls below the cavitation pressure threshold. Therefore, we consider the risk of outside cavitation to be relatively small, especially for apical sizes ISO 10 to 40.

Another crucial safety consideration associated with any irrigation is the extrusion of the irrigant through the apical constriction, which can cause serious complications. The highest risk represents the chemical action of the extruded irrigant with the tissue and nerves, while the risk of bacteria getting expelled into the surrounding tissue is minimized because of the bactericidal effect of the irrigant. Apical extrusion studies [10,19,29,30], have shown that the extrusion during LAI, including when using the SWEEPS technique [31], is smaller in comparison with conventional irrigation techniques such as needle and ultrasonic irrigation. However, further research is recommended to evaluate extrusion during SWEEPS irrigation under the enhanced pressure conditions.

Finally, it is worth noting that recently published studies with novel laser systems [32–34] suggest that laser ablation may be used also as an alternative to standard mechanical instrumentation in order to reduce generated debris and smear layer.

CONCLUSIONS

Laser-induced cavitation dynamics in constrained canals was examined with two measuring techniques.

A high-speed camera was used to observe the life cycle of a cavitation bubble, where its maximal diameter and oscillation time were measured. A second measuring system was used for internal pressure measurement, where the principle of water level difference was used to measure time-average pressures at five regions within the model of the root canal.

Our study shows that internal pressure can be increased by a factor of 1.5 by using double Er:YAG laser pulses if they are optimally separated. The results show that for the pressure increase the separation time must approximately coincide with the single bubble oscillation time. Similar condition was found also for the generation of shock waves in spatially confined cavities [22].

Therefore, if the SWEEPS method is to be used in a wide spectrum of canal sizes, the relation between the bubble oscillation time and canal size must be known. We found good correlation ($R^2 = 0.96$) between normalized oscillation time and canal diameter for a wide range of laser pulse energies. This means that we can determine the bubble oscillation time within a constrained volume if the oscillation time in infinite space is known. The practicability of this finding is in the fact that the oscillation time is much easier to measure *in vitro* in a large fluid reservoir using an optical method in comparison with *in vivo* techniques.

Our results also show good correlation ($R^2 = 0.90$) between average pressure within the canal and the bubble oscillation periods. This offers a new method of laser parameter optimization by simply measuring the bubble oscillation periods within the same cavity. The parameter combination, which results in the longest bubble oscillation period will be most effective also for pressure generation.

These findings enable determination of optimal conditions for shock wave generation, and improvement of root canal irrigation at the same dose of laser energy input. Although only root canal treatments were considered in this study, our findings may be of benefit also for other medical procedures based on cavitation phenomena, such as fragmentation of urinary stones in laser lithotripsy [35], or removal of arterial blood clots in laser thrombolysis [36].

ACKNOWLEDGMENTS

This research was supported by the Ministry of Education, Science and Sport, Slovenia, under grants L3-7658, P2-0392, and Fotona d.o.o.

REFERENCES

1. Peters OA. Current challenges and concepts in the preparation of root canal systems: A review. *J Endod* 2004;30(8): 559–567.
2. Peters OA, Schönenberger K, Laib A. Effects of four Ni-Ti preparation techniques on root canal geometry assessed by micro computed tomography. *Int Endod J* 2001;34(3): 221–230.
3. Hülsmann M, Rummelin C, Schäfers F. Root canal cleanliness after preparation with different endodontic handpieces

- and hand instruments: A comparative SEM investigation. *J Endod* 1997;23(5):301–306.
4. Akcay M, Arslan H, Mese M, Durmus N, Capar ID. Effect of photon-initiated photoacoustic streaming, passive ultrasonic, and sonic irrigation techniques on dentinal tubule penetration of irrigation solution: A confocal microscopic study. *Clin Oral Investig* 2017;21(7):2205–2212.
 5. Ahmad M, Pitt Ford TR, Crum LA, Walton AJ. Ultrasonic debridement of root canals: Acoustic cavitation and its relevance. *J Endod* 1988;14(10):486–493.
 6. de Gregorio C, Estevez R, Cisneros R, Paranjpe A, Cohenca N. Efficacy of different irrigation and activation systems on the penetration of sodium hypochlorite into simulated lateral canals and up to working length: An in vitro study. *J Endod* 2010;36(7):1216–1221.
 7. Charara K, Friedman S, Sherman A, et al. Assessment of apical extrusion during root canal irrigation with the novel gentlewave system in a simulated apical environment. *J Endod* 2016;42(1):135–139.
 8. Bryce G, MacBeth N, Gulabivala K, Ng Y-L. The efficacy of supplementary sonic irrigation using the EndoActivator® system determined by removal of a collagen film from an ex vivo model. *Int Endod J* 2018;51(4):489–497.
 9. Vyas N, Manmi K, Wang Q, et al. Which parameters affect biofilm removal with acoustic cavitation? A review. *Ultrasound Med Biol* 2019;45(5):1044–1055.
 10. George R, Walsh LJ. Apical extrusion of root canal irrigants when using Er:YAG and Er,Cr:YSGG lasers with optical fibers: An in vitro dye study. *J Endod* 2008;34(6):706–708.
 11. Lukac N, Zadavec J, Gregorcic P, Lukac M, Jezeršek M. Wavelength dependence of photon-induced photoacoustic streaming technique for root canal irrigation. *J Biomed Opt* 2016;21(7):75007.
 12. George AM, Kalangi SK, Vasudevan M, Krishnaswamy NR. Chlorhexidine varnishes effectively inhibit *Porphyromonas gingivalis* and *Streptococcus mutans*—An in vivo study. *J Indian Soc Periodontol* 2010;14(3):178–180.
 13. Lukač N, Gregorčič P, Jezeršek M. Optodynamic phenomena during laser-activated irrigation within root canals. *Int J Thermophys* 2016;37(7):66.
 14. Blanken J, De Moor RJ, Meire M, Verdaasdonk R. Laser induced explosive vapor and cavitation resulting in effective irrigation of the root canal. Part 1: A visualization study. *Lasers Surg Med* 2009;41(7):514–519.
 15. de Groot SD, Verhaagen B, Versluis M, Wu M-K, Wesselink PR, van der Sluis LWM. Laser-activated irrigation within root canals: Cleaning efficacy and flow visualization. *Int Endod J* 2009;42(12):1077–1083.
 16. Koch JD, Jaramillo DE, DiVito E, Peters OA. Irrigant flow during photon-induced photoacoustic streaming (PIPS) using particle image velocimetry (PIV). *Clin Oral Investig* 2016;20(2):381–386.
 17. Matsumoto H, Yoshimine Y, Akamine A. Visualization of irrigant flow and cavitation induced by Er:YAG laser within a root canal model. *J Endod* 2011;37(6):839–843.
 18. Olivi G, DiVito E. Photoacoustic endodontics using PIPS: Experimental background and clinical protocol. *J Laser Health Acad* 2012;2012(1):1–7.
 19. Arslan D, Kustarci A. Efficacy of photon-initiated photoacoustic streaming on apically extruded debris with different preparation systems in curved canals. *Int Endod J* 2018; 51(Suppl 1):e65–e72.
 20. Galler KM, Grubmüller V, Schlichting R, et al. Penetration depth of irrigants into root dentine after sonic, ultrasonic and photoacoustic activation. *Int Endod J* 2019;52(8): 1210–1217.
 21. Šarc A, Kosel J, Stopar D, Oder M, Dular M. Removal of bacteria *Legionella pneumophila*, *Escherichia coli*, and *Bacillus subtilis* by (super)cavitation. *Ultrason Sonochem* 2018;42:228–236.
 22. Lukač N, Jezeršek M. Amplification of pressure waves in laser-assisted endodontics with synchronized delivery of Er:YAG laser pulses. *Lasers Med Sci* 2018;33(4):823–833.
 23. Gregorčič P, Lukač N, Možina J, Jezeršek M. Synchronized delivery of Er:YAG-laser pulses into water studied by a laser beam transmission probe for enhanced endodontic treatment. *Appl Phys A: Mater Sci Process* 2016; 122(4):459.
 24. Lukac N, Tasic Muc B, Jezersek M, Lukac M. Photoacoustic endodontics using the novel SWEEPS Er:YAG laser modality. *J Laser Health Acad* 2017;2017(1):1–7.
 25. Ostadfar A. *Biofluid Mechanics: Principles and Applications*. Amsterdam: Elsevier/Academic Press; 2016.
 26. Fu J, Li Z, Li N. Hagen-Poiseuille equation: A non-invasive tool for detecting renal pelvic pressure. *Biomed Res* 2017; 28(6):2865–2869.
 27. Gregorčič P, Jezeršek M, Možina J. Optodynamic energy-conversion efficiency during an Er:YAG-laser-pulse delivery into a liquid through different fiber-tip geometries. *J Biomed Opt* 2012;17(7):0750061.
 28. Brujan EA, Williams PR. Bubble dynamics and cavitation in non-Newtonian liquids. *Rheol Rev* 2005;2005:147–172.
 29. Genc SO, Kaya M. Comparative safety of needle, EndoActivator, and Laser-activated irrigation in overinstrumented root canals. *Photomed Laser Surg* 2018;36:198–202.
 30. Fukumoto Y. Intracanal aspiration technique for root canal irrigation: Evaluation of smear layer removal. *Kokubyo Gakkai Zasshi* 2005;72(1):13–18.
 31. Jezersek M, Jereb T, Lukac N, Tenyi A, Lukac M, Fidler A. Evaluation of apical extrusion during novel Er:YAG laser-activated irrigation modality. *Photobiomodul Photomed Laser Surg* 2019;37(9):544–550.
 32. Fried WA, Chan KH, Darling CL, Curtis DA, Fried D. Image-guided ablation of dental calculus from root surfaces using a DPSS Er:YAG laser. *Lasers Surg Med* 2019. <https://doi.org/10.1002/lsm.23122>
 33. Loganathan S, Santhanakrishnan S, Bathe R, Arunachalam M. Surface processing: An elegant way to enhance the femtosecond laser ablation rate and ablation efficiency on human teeth. *Lasers Surg Med* 2019;51:797–807.
 34. Berg BI, Peyer M, Kuske L, et al. Comparison of an Er: YAG laser osteotome versus a conventional drill for the use in osteo-odonto-keratoprosthesis (OOKP). *Lasers Surg Med* 2019;51:531–537.
 35. Vassar G, Chan K, Teichman J, et al. Holmium: Yag lithotripsy: Photothermal mechanism. *J Endourol* 1999;13: 181–190.
 36. Yuan F, Sankin G, Zhong P. Dynamics of tandem bubble interaction in a microfluidic channel. *J Acoust Soc Am* 2011;130:3339–3346.